Available online at www.sciencedirect.com
ScienceDirect
Journal of Photochemistry and Photobiology A: Chemistry 190 (2007) 274–282
Journal of Photochemistry and Photobiology A:Chemistry
www.elsevier.com/locate/jphotochem

The MP/SOFT methodology for simulations of quantum dynamics: Model study of the photoisomerization of the retinyl chromophore in visual rhodopsin

Xin Chen, Victor S. Batista *

Department of Chemistry, Yale University, P.O. Box 208107, New Haven, CT 06520-8107, United States

Available online 18 May 2007

Abstract

Rigorous simulations of excited-state nonadiabatic quantum dynamics in polyatomic chromophores are particularly challenging since they require solving the multichannel time-dependent Schrödinger equation describing nuclear wavepackets evolving on electronically coupled potential energy surfaces. This paper presents an overview of the matching-pursuit/split-operator-Fourier-transform (MP/SOFT) method for simulations of nonadiabatic quantum dynamics [X. Chen, V.S. Batista, Matching-pursuit split operator Fourier transform simulations of excited-state nonadiabatic quantum dynamics in pyrazine. J. Chem. Phys., 125 (2006) Art. No. 124313] and its application to the description of the 11-*cis*/all-*trans* photoisomerization of the retinyl chromophore in rhodopsin. The underlying nonadiabatic dynamics is described by a 2-state 25-dimensional wave-packet evolving according to an empirical model Hamiltonian with frequencies and excited-state gradients parameterized to reproduce the observed resonance Raman excitations of rhodopsin. The reported results show that the MP/SOFT method is a valuable tool to simulate nonadiabatic dynamics in polyatomic systems and to assess the validity of mixed quantum-classical approaches as applied to simulations of complex (nonintegrable) quantum dynamics in multidimensional systems.

Keywords: Quantum dynamics; Rhodopsin; Photoisomerization; Nonadiabatic; Retinal; Ultrafast phenomena

1. Introduction

Understanding ultrafast photoinduced reactions in excited electronic states of polyatomic chromophores is a problem common to a wide range of systems in chemistry, biology, physics and beyond. Many experimental techniques implementing ultrafast time-resolved pump-probe spectroscopy (besides various types of transient absorption experiments) have been developed to study a variety of ultrafast photoinduced processes, including isomerization reactions, excited state intramolecular proton transfer, direct dissociation, vibrational energy redistribution and electronic internal conversion, among others. The unambiguous interpretation of these highly multiplexed pump-probe experiments, however, often requires theoretical simulations since the signals result from complicated nonadiabatic dynamics involving multiple potential energy surfaces (PESs). This paper presents an overview of the matching-pursuit/split-operator-Fourier-transform (MP/SOFT) method for simulations of nonadiabatic quantum dynamics [1] and its illustration as applied to modeling the ultrafast 11-*cis*/all-*trans* photoisomerization of the retinyl chromophore in rhodopsin, described by the structural diagram of Fig. 1.

The photoisomerization of the retinyl chromophore in rhodopsin constitutes the primary step in the vertebrate vision process [2–9] and has been the subject of extensive experimental and theoretical studies. Femtosecond pump-probe spectroscopic measurements have provided detailed time-resolved information on the photoisomerization and interconversion dynamics, indicating that the all-*trans* photoproduct is formed within 200 fs with high efficiency (67%) [10–12]. However, due to the complexity of the problem, the complete theoretical description of the underlying nonadiabatic dynamic has yet to be reported with an explicit treatment of the rhodopsin environment. In this paper, the description of dynamics is based on an approximate empirical model Hamiltonian with frequencies and excited-state gradients parameterized to reproduce the observed resonance Raman excitations of rhodopsin.

Most previous theoretical studies were performed long before the crystallographic structure of rhodopsin was available [13–18]. However, the recently reported X-ray crystal

* Corresponding author. Tel.: +1 203 432 6672; fax: +1 203 432 6144.
E-mail address: victor.batista@yale.edu (V.S. Batista).

1010-6030/$ – see front matter © 2007 Elsevier B.V. All rights reserved.
doi:10.1016/j.jphotochem.2007.05.015

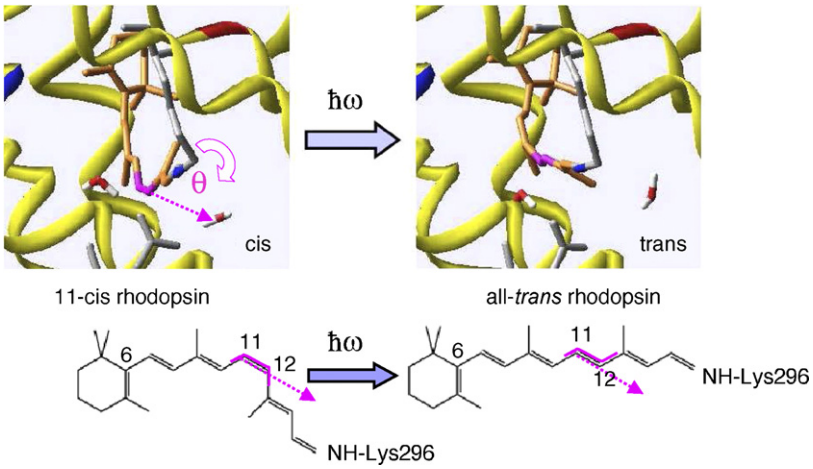

Fig. 1. Structural diagram of the 11-*cis*/all-*trans* photoisomerization of the retinyl chromophore in visual rhodopsin. The C_{11}–C_{12} bond and the dihedral angle $\theta(C_{11}–C_{12})$ are highlighted in magenta.

structures of bovine rhodopsin [19–21] have motivated several computational studies that focused on the analysis of the geometry and electronic excitation of the retinyl chromophore [22–26], the underlying molecular rearrangements, and the mechanism of energy storage by 11-*cis*/all-*trans* isomerization [27–31]. In addition, several studies based on reduced dimensional model systems have investigated the underlying nonadiabatic dynamics associated with the photoisomerization of the chromophore [32–37], including studies based on approximate mixed quantum-classical techniques applied in conjunction with an empirical 2-state 2-mode model Hamiltonian, coupled to a classical bath of 23 vibrational modes of rhodopsin [38,39]. This model Hamiltonian is thus particularly suited for detailed investigations based on newly developed computational methods since it allows for direct comparisons with previous studies and recent theoretical work on related systems [40,41]. This paper reports simulations of the photoisomerization dynamics treating the 2-state 25-mode model fully quantum mechanically. This includes the two coordinates accounting for the collective torsion about the C_{11}–C_{12} bond and its coupling to the delocalized stretching mode of the polyene chain, evolving on 2 electronically coupled potential energy surfaces. The quantum bath includes 23 vibrational modes with frequencies and excited-state gradients parameterized to reproduce the experimental resonance Raman excitations of rhodopsin [42].

Numerically exact simulations of excited-state nonadiabatic quantum dynamics are particularly challenging since they require solving the multi-channel time-dependent Schrödinger equation for the description of nuclear motion on multiple coupled potential energy surfaces. This problem can be rigorously solved by applying methods for wave-packet propagation [43–55], such as approaches based on the split-operator-Fourier transform (SOFT) method [56–58], the Chebyshev expansion [59] and the short iterative Lanczos algorithms [60]. While rigorous, these approaches demand storage space and computational effort that scale exponentially with the number of coupled degrees of freedom in the system, limiting their applicability to molecular systems with very few atoms (e.g., less than three or four atoms). Due to this scalability problem, studies of nonadiabatic dynamics in polyatomic systems have been usually based on approximate methods built around semi-classical and mixed quantum-classical treatments [61–75]. However practical, these popular mixed quantum-classical approaches rely upon *ad hoc* approximations whose resulting consequences are often difficult to quantify in applications to complex (*i.e.*, nonintegrable) dynamics. It is, thus, imperative to develop practical, yet rigorous, methods to validate approximate approaches and gain insight into the nature of quantum dynamics [1,76–87].

The MP/SOFT method [1,82–87] is a time-dependent propagation scheme for numerically exact simulations of quantum processes. The method is based on the propagation of multidimensional time-dependent wave-packets, represented in matching-pursuit coherent-state expansions, by analytically applying the time-evolution operator as defined by the Trotter expansion to second order accuracy. The resulting propagation scheme thus bypasses the 'exponential scaling problem' of the standard grid-based SOFT approach [56–58], usually limited by the capabilities of the fast-Fourier transform FFT algorithm [88]. Furthermore, the MP/SOFT method overcomes the 'truncation problem', natural to propagation schemes where the basis set is defined *a priori*, by dynamically adapting the coherent-state expansion according to the desired propagation accuracy. When compared to alternative time-dependent methods, including the MCTDH method [89,90] and approaches based on coherent-state expansions [78,79,91–105], the MP/SOFT method is usually easier to implement since it has the advantage of avoiding the need of propagating time-dependent expansion coefficients, a task that would require solving a coupled system of differential equations. The main drawback of the MP/SOFT method is that it requires generating a new coherent-state expansion for each propagation step. However, such a computational task can be trivially parallelized, overcoming the limitations of memory/storage bandwidth in terms of readily available computational processing power.

The accuracy and efficiency of the MP/SOFT method have already been demonstrated in several applications to multidimensional quantum dynamics, including recent studies

of the excited-state intramolecular proton transfer in 2-(2′-hydroxyphenyl)-oxazole [87], as modeled by the propagation of a 35-dimensional wave packet; and the S_1/S_2 interconversion of pyrazine after $S_0 \rightarrow S_2$ photoexcitation, as modeled by the propagation of a 24-dimensional wave-packet undergoing nonadiabatic dynamics at the S_1/S_2 conical intersection of potential energy surfaces [1]. This paper shows that the same methodology can be efficiently implemented to simulate the nonadiabatic dynamics of the retinyl chromophore in rhodopsin, after $S_0 \rightarrow S_1$ photoexcitation, by propagating a 25-dimensional wave-packet evolving according to an empirical 2-state 25-mode model Hamiltonian.

The paper is organized as follows. Section 2 describes the MP/SOFT methodology for simulations of nonadiabatic quantum dynamics and the 2-state 25-mode model Hamiltonian used for the description of the 11-*cis*/all-*trans* photoisomerization in rhodopsin. Section 3 presents results of calculations of the time-dependent populations associated with the 11-*cis* and all-*trans* configurations and the analysis of the time-dependent wave-packet as a function of the isomerization coordinate and the generalized stretching mode of the chromophore polyene chain. Section 4 summarizes and concludes.

2. Methods

2.1. MP/SOFT method

Consider the simulation of nonadiabatic quantum dynamics according to the 2-state model Hamiltonian:

$$\hat{H} = \frac{\hat{p}^2}{2m} + \hat{V}, \tag{1}$$

where $\hat{V} = \hat{V}_0 + \hat{V}_c$ with $\hat{V}_0 = V_1(\hat{\mathbf{x}})|1\rangle\langle 1| + V_2(\hat{\mathbf{x}})|2\rangle\langle 2|$ and $\hat{V}_c = V_c(\hat{\mathbf{x}})|1\rangle\langle 2| + V_c(\hat{\mathbf{x}})|2\rangle\langle 1|$. Here, $\boldsymbol{x} = (\theta, x_{str}, z_j)$ represents the nuclear coordinates, collectively, including the torsional coordinate θ; the delocalized stretching mode of the polyene chain, x_{str} and the Condon-active vibrational modes z_j of rhodopsin, as specified in Section 2.3. The computational task ahead involves obtaining the time-dependent wave-packet:

$$|\Psi(\mathbf{x};t)\rangle = \varphi_1(\mathbf{x};t)|1\rangle + \varphi_2(\mathbf{x};t)|2\rangle, \tag{2}$$

where, $\varphi_1(\mathbf{x};t)$ and $\varphi_2(\mathbf{x};t)$ are the nuclear wave-packet components associated with the diabatic electronic states, $|1\rangle$ and $|2\rangle$, as determined by the evolution of the initial states:

$$\varphi_1(\mathbf{x};0) = 0, \qquad \varphi_2(\mathbf{x};0) = \prod_{j=1}^{N}\left(\frac{1}{\pi}\right)^{1/4} e^{-x(j)^2/2}, \tag{3}$$

associated with the S_0 and S_1 states, respectively. Here, $N = 25$ is the dimensionality of the system, as defined by the number of nuclear coordinates explicitly considered in the model Hamiltonian.

A simple propagation scheme would require representing the initial states $\varphi_1(\mathbf{x};0)$ and $\varphi_2(\mathbf{x};0)$ in a convenient nuclear basis set and propagating $\varphi_1(\mathbf{x};t)$ and $\varphi_2(\mathbf{x};t)$ by applying the time-evolution operator, e.g., as defined by the embedded form of the Trotter expansion:

$$\begin{aligned} e^{-i\hat{H}2\tau} &\approx e^{-i(\hat{p}^2/2m)\tau}\, e^{-iV(\hat{\mathbf{x}})2\tau}\, e^{-i(\hat{p}^2/2m)\tau} \\ &\approx e^{-i(\hat{p}^2/2m)\tau}\, e^{-iV_0(\hat{\mathbf{x}})\tau}\, e^{-iV_c(\hat{\mathbf{x}})2\tau}\, e^{-iV_0(\hat{\mathbf{x}})\tau}\, e^{-i(\hat{p}^2/2m)\tau}. \end{aligned} \tag{4}$$

Working in the basis set of electronic states $|1\rangle$ and $|2\rangle$, this can be accomplished according to the following steps:

- Step [I]. Apply the free-particle propagator to both wave-packet components $\varphi_1(\mathbf{x};t)$ and $\varphi_2(\mathbf{x};t)$ for time τ, as follows:

$$\begin{pmatrix} \varphi_1'(\mathbf{x};t+\tau) \\ \varphi_2''(\mathbf{x};t+\tau) \end{pmatrix} = \begin{pmatrix} e^{-i(\hat{\boldsymbol{p}}^2/2m)\tau} & 0 \\ 0 & e^{-i(\hat{\boldsymbol{p}}^2/2m)\tau} \end{pmatrix} \times \begin{pmatrix} \varphi_1(\mathbf{x};t) \\ \varphi_2(\mathbf{x};t) \end{pmatrix}. \tag{5}$$

- Step [II]. Mix the two wave-packet components $\varphi_1'(\mathbf{x};t+\tau)$ and $\varphi_2'(\mathbf{x};t+\tau)$:

$$\begin{pmatrix} \varphi_1''(\mathbf{x};t+\tau) \\ \varphi_2''(\mathbf{x};t+\tau) \end{pmatrix} = \mathbf{M} \begin{pmatrix} \varphi_1'(\mathbf{x};t+\tau) \\ \varphi_2'(\mathbf{x};t+\tau) \end{pmatrix}, \tag{6}$$

with

$$\mathbf{M} \equiv \mathbf{L}^{-1} \begin{pmatrix} e^{-iE_1(x)\tau} & 0 \\ 0 & e^{-iE_2(x)\tau} \end{pmatrix} \mathbf{L}, \tag{7}$$

where $E_1(x)$ and $E_2(x)$ are the eigenvalues of the potential energy matrix $V = V_0 + V_c$ and $\mathbf{L}$ is the matrix of column eigenvectors in the basis of diabatic states $|1\rangle$ and $|2\rangle$. The specific case of interest involves a 2×2 Hermitian matrix V. Therefore, the matrix $\mathbf{M}$ can be *analytically* obtained as described in Ref. [1]:

$$\mathbf{M} \equiv \begin{pmatrix} \cos(2V_c(\hat{\mathbf{x}})\tau)\, e^{-i\hat{V}_1(\hat{\mathbf{x}})2\tau} & -i\,\sin(2V_c(\hat{\mathbf{x}})\tau)\, e^{-i(\hat{V}_1(\hat{\mathbf{x}})+V_2(\hat{\mathbf{x}}))\tau} \\ -i\,\sin(2V_c(\hat{\mathbf{x}})\tau)\, e^{-i(\hat{V}_1(\hat{\mathbf{x}})+V_2(\hat{\mathbf{x}}))\tau} & \cos(2V_c(\hat{\mathbf{x}})\tau)\, e^{-i\hat{V}_2(\hat{\mathbf{x}})2\tau} \end{pmatrix}. \tag{8}$$

Step [III]. Propagate $\varphi_1''(\mathbf{x};t+\tau)$ and $\varphi_2''(\mathbf{x};t+\tau)$ for time τ, according to the free-particle propagator by applying the kinetic energy part of the Trotter expansion:

$$\begin{pmatrix} \varphi_1(\mathbf{x};t+2\tau) \\ \varphi_2(\mathbf{x};t+2\tau) \end{pmatrix} = \begin{pmatrix} e^{-i(\hat{p}^2/2m)\tau} & 0 \\ 0 & e^{-i(\hat{p}^2/2m)\tau} \end{pmatrix} \times \begin{pmatrix} \varphi_1''(\mathbf{x};t+\tau) \\ \varphi_2''(\mathbf{x};t+\tau) \end{pmatrix}. \tag{9}$$

In practice, Step [III] is combined with Step [I] of the next propagation time-slice for all but the last propagation time-increment.

In the usual grid-based implementation of this approach, Step [I] requires Fourier transforming states $\varphi_l(\mathbf{x};t)$ to the momentum representation, multiplying the transform-states by the free

particle propagator $e^{-i(p^2/2m)\tau}$, and then inverse-Fourier transforming the product, back to the coordinate representation. This standard grid-based procedure would be computationally intractable for the present application since it would be limited by the exponential scaling of the fast-Fourier transform FFT algorithm [88]. Such computational difficulties are by-passed in the MP/SOFT approach by representing states $\varphi_l(\boldsymbol{x};\, t)$ as matching-pursuit coherent-state expansions (see Section 2.2):

$$\varphi_l(\mathbf{x};t) \approx \sum_{j=1}^{N} c_j^{(l)} \langle \mathbf{x}|\chi_j\rangle, \tag{10}$$

where $\langle \boldsymbol{x}|\chi_j\rangle$ are N-dimensional coherent-states:

$$\langle \mathbf{x}|\chi_j\rangle \equiv \prod_{k=1}^{N} A_j(k)\, \exp\left(-\frac{\gamma_j(k)}{2}(\boldsymbol{x}(k)-\boldsymbol{x}_j(k))^2 + ip_j(k)(x(k)-xj_{(k)})\right), \tag{11}$$

with normalization factors $A_j(k)$ and complex-valued parameters $\gamma_j(k)$, $x_j(k)$ and $p_j(k)$ selected, as described in Section 2.2. The expansion coefficients $c_j^{(l)}$, introduced by Eq. (10), are defined according to the matching pursuit algorithm [106], as follows: $c_j^{(l)} \equiv \langle \chi_1|\varphi_l\rangle$ and $c_j^{(l)} \equiv \langle \chi_j|\varphi_l\rangle - \sum_{k=1}^{j-1} c_k^{(l)} \langle \chi_j|\chi_k\rangle$, for $j = 2-N$.

The coherent-state expansions, introduced by Eq. (10), allow for the *analytic* implementation of step [1] as follows:

$$\varphi_l'(\mathbf{x};t+\tau) = \sum_{j=1}^{n} c_j^{(l)} \langle \mathbf{x}|\tilde{\chi}_j\rangle, \tag{12}$$

where

$$\langle \mathbf{x}|\tilde{\chi}_j\rangle \equiv \prod_{k=1}^{N} A_j(k) \sqrt{\frac{m}{m+i\tau\gamma_j(k)}} \exp\left(\frac{(p_j(k)/\gamma_j(k)) - i[x_j(k)-x(k)]^2}{(2/\gamma_j(k)) + (2i\tau/m)} - \frac{p_j(k)}{2\gamma_j(k)}\right). \tag{13}$$

Step [II] is efficiently implemented by generating matching pursuit coherent-state expansions of $\varphi_l''(\mathbf{x};\, t+\tau)$, as described in Section 2.2. Here, we use the definition of $\mathbf{M}$, introduced by Eq. (8), in addition to the coherent-state expansions of $\varphi_l'(\mathbf{x};\, t+\tau)$, introduced by Eq. (12) and the specific functional form of the model potential energy surfaces introduced in Section 2.3.

2.2. Matching pursuit expansions

The matching pursuit coherent state expansions, representing target states Ψ_t (wave-functions), are obtained by successive orthogonal projections onto elements of an over-complete basis set as follows: The first step requires selecting the basis element $|1\rangle$ that has maximum overlap with the target state $|\Psi_t\rangle$ (*i.e.*, the element that is resonant with the most prominent structure in $|\Psi_t\rangle$). The first order expansion is thus defined as follows:

$$|\psi_t\rangle = c_1|1\rangle + |\varepsilon_1\rangle, \tag{14}$$

where $c_1 \equiv \langle 1|\Psi_t\rangle$. Note that the residual vector $|\varepsilon_1\rangle$ is orthogonal to $|1\rangle$. Therefore, $||\Psi_t|| > ||\varepsilon_1||$, by virtue of the definition of c_1. The next step involves the sub-decomposition of the residual vector $|\varepsilon_1\rangle$ by projecting it along the direction of its best match $|2\rangle$ as follows:

$$|\varepsilon_1\rangle = c_2|2\rangle + |\varepsilon_2\rangle, \tag{15}$$

where $c_2 \equiv \langle 2|\varepsilon_1\rangle$. Note that, since $|\varepsilon_1\rangle$ is orthogonal to $|2\rangle$, the norm of $|\varepsilon_2\rangle$ is smaller than the norm of $|\varepsilon_1\rangle$. This procedure is repeated each time on the resulting residue.

After n successive orthogonal projections, the norm of the residual vector $|\varepsilon_n\rangle$ is smaller than a desired precision ε. Therefore, the algorithm maintains norm conservation within a desired precision:

$$||\varepsilon_n|| = \sqrt{1 - \sum_{j=1}^{n} |c_j|^2} < \varepsilon, \tag{16}$$

just as in a linear orthogonal decomposition. The resulting expansion is

$$\langle x|\psi_t\rangle \approx \sum_{j=1}^{n} c_j \langle \mathbf{x}|j\rangle, \tag{17}$$

where the coefficients c_j are recursively defined as follows:

$$c_j = \langle j|\psi_t\rangle - \sum_{k=1}^{j-1} c_k \langle j|k\rangle. \tag{18}$$

A discussion of convergence with respect to the number of basis states and the numerical effort required in typical MP/SOFT simulations has been previously reported [1,84,87]. Matching pursuit coherent-state expansions are obtained by successively selecting the basis functions according to a gradient-based optimization technique [88]. A parallel implementation under the message passing interface (MPI) environment [107] can linearly accelerate the search for a satisfactory local minimum, with the number of processing elements. Starting from an initial trial coherent state $|\chi\rangle$, the parameters $x_j(k)$, $p_j(k)$ and $\gamma_j(k)$ are optimized so that they locally maximize the overlap with the target state. Initial guess parameters $\gamma_j(k)$, $x_j(k)$ and $p_j(k)$ are chosen as defined by the basis elements of the previous wave-packet representation (or initial state).

2.3. Model Hamiltonian

A detailed description of the model Hamiltonian, implemented for the reported MP/SOFT simulations, has been previously reported [38,39,108–110]. Here, the model is described only briefly.

The model involves an empirical 2-state 25-mode Hamiltonian $H = H_M + H_B$, where H_M is a 2-state 2-mode model Hamiltonian that explicitly accounts for the collective torsional

coordinate θ and its coupling to the delocalized stretching mode of the polyene chain x_{str}, as follows:

$$H_M = \sum_{n,m=1,2} |n\rangle(T\delta_{nm} + V_{nm})\langle m|, \tag{19}$$

where

$$T = -\frac{1}{2m}\frac{\partial^2}{\partial\theta^2} - \frac{\omega}{2}\frac{\partial^2}{\partial x_{str}^2}, \tag{20}$$

$$V_{nn} = V_n^R(\theta) + \tfrac{1}{2}\omega x_{str}^2 + \delta_{2n}kx_{str}, \tag{21}$$

$$V_{12} = V_{21} = \lambda x_{str}, \tag{22}$$

$$V_1^R = \tfrac{1}{2}W_1(1 - \cos(\theta)), \tag{23}$$

$$V_2^R = E_2 - \tfrac{1}{2}W_2(1 - \cos(\theta)), \tag{24}$$

assuming dimensionless coordinates and atomic units (with $\hbar = 1$). The parameters of the model are defined as follows: $m^{-1} = 4.84 \times 10^{-4}$ eV, $E_2 = 2.48$ eV, $W_1 = 3.6$ eV, $W_2 = 1.09$ eV, $\omega = 0.19$ eV, $\kappa = 0.1$ eV and $\lambda = 0.19$ eV, in order to reproduce the rhodopsin electronic excitation energies as well as the spectroscopic energy shift and energy storage due to the isomerization of the retinyl chromophore in rhodopsin. Therefore, the model implicitly considers the effect of the protein environment in the actual values of the parameters. Fig. 2 shows the resulting adiabatic potential energy surfaces obtained by diagonalization of V_{nm}.

The condon-active vibrational modes z_j are included as a harmonic ansatz:

$$H_B = \sum_{n=1,2} |n\rangle\langle n| \sum_j \frac{1}{2}\omega_j(p_j^2 + z_j^2) + \delta_{n2}\alpha_j z_j, \tag{25}$$

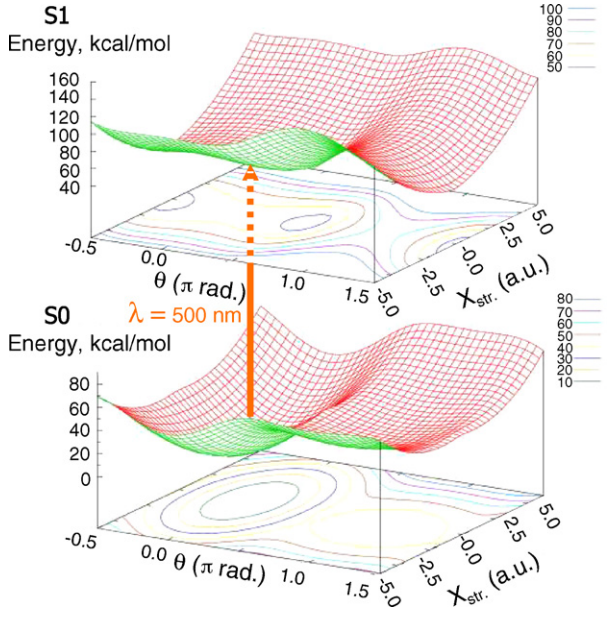

Fig. 2. Adiabatic potential energy surfaces for the ground (S_0) and excited (S_1) electronic states, as a function of the isomerization dihedral angle $\theta(C_{11}$–$C_{12})$ and the delocalized stretching mode x_{str} of the polyene chain. The vertical arrow indicates the preparation of the initial states by $S_0 \rightarrow S_1$ photoexcitation with visible-light ($\lambda = 500$ nm).

with frequencies ω_j and excited-state gradients α_j parameterized to reproduce the experimental resonance Raman excitations of rhodopsin [42]. In addition to reproducing all of these experimental data by construction, the model Hamiltonian properly describes the isomerization reaction rate and efficiency (*i.e.*, the quantum product yield) [38], as correlated to femtosecond spectroscopic signals [10–12].

3. Results

This section demonstrates the capabilities of the generalized MP/SOFT method, introduced in Section 2, as applied to the description of the 11-*cis*/all-*trans* isomerization of the retinyl chromophore in rhodopsin. Benchmark calculations showing the accuracy and efficiency of the generalized MP/SOFT method, as compared to numerically exact grid-based computations, have already been reported [1]. The isomerization involves ultrafast nonadiabatic dynamics at the S_0/S_1 conical intersection of potential energy surfaces.

Fig. 3 shows the evolution of the time dependent wave-packet, reduced to the space of reaction coordinates θ and x_{str} as follows:

$$\rho_t(\theta, x_{str}) = \int dz |\psi_t^*(\theta, x_{str}, z)|^2, \tag{26}$$

and represented by solid contour lines. Snapshots at various times, during the nonadiabatic dynamics following the $S_0 \rightarrow S_1$ photoexcitation of the retinyl chromophore, illustrate the process of excited-state relaxation at the detailed molecular level. Initially, the wave-packet spreads in the S_1 state and approaches the S_1/S_0 conical intersection of potential energy surfaces, at $\theta = \pi/2$ rad and $x_{str} = 0$ a.u. within 100 fs. During this first encounter with the conical intersection, there is population transfer from the S_1 electronic state to highly excited rovibrational states associated with the *trans* configuration of the retinyl chromophore in the S_0 electronic state. This scattering process induces vibrational energy redistribution, at the conical intersection, exciting both the torsional motion about the C_{11}–C_{12} bond and the delocalized stretching mode of the polyene chain for the chromophore in both the S_0 and S_1 states (see snapshot at $t = 150$ fs). The subsequent relaxation dynamics involves ground-state relaxation into highly excited vibronic states of the *cis* configuration as well as further population transfer from the S_1 state into the *trans* configuration of the S_0 state.

Fig. 4 shows the evolution of the time-dependent population of the retinyl chromophore in the 11-*cis* S_1 adiabatic state, $P_{cis}^{S_1}(t) = \langle \Psi^{S_1}(t)|h(\theta)|\Psi^{S_1}|(t)\rangle$, where $|\Psi^{S_1}(t)\rangle = \langle S_1|\Psi(t)\rangle|S_1\rangle$, and the population of the all-*trans* S_0 adiabatic state, $P_{trans}^{S_0}(t)$, obtained analogously during the early time dynamics after photoexcitation of the system. Here, $\Psi(t)$ is the 2-state time-dependent wave-packet introduced by Eq. (2) and $h(\theta)$ is a step-function of the dihedral angle θ about the C_{11}–C_{12} bond, defined as follows: $h(\theta) = 1$, when $|\theta| < \pi/2$ and $h(\theta) = 0$, otherwise. MP/SOFT results (solid lines) are compared to the corresponding calculations obtained according to the mixed quantum-classical time-dependent self-consistent field (TDSCF) approach [63] (dashed lines), implemented as described in Ref. [39].

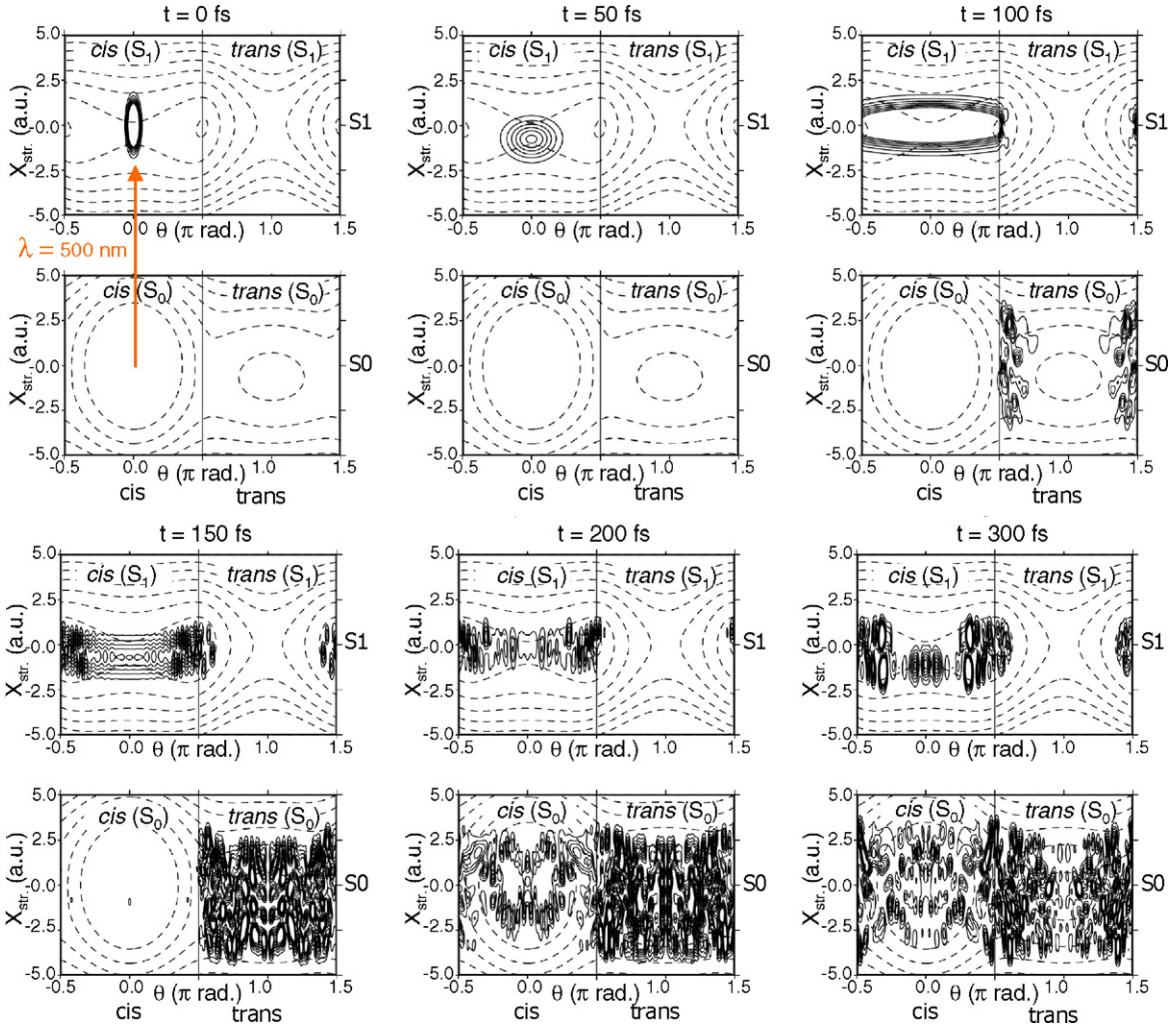

Fig. 3. Evolution of the time-dependent wave-packet $\rho_t(\theta, x_{str}) = \int dz|\Psi_t^*(\theta, x_{str}, z)|^2$, reduced to the space of reaction coordinates θ and x_{str}, at various different times during the nonadiabatic dynamics following $S_0 \rightarrow S_1$ photoexcitation of the retinyl chromophore. Wavepackets are represented by solid contour lines, equally spaced by 0.1 units in the 0.1–0.7 range of amplitudes. The S_0 and S_1 states are represented by broken contour lines.

Fig. 4 shows that the product all-*trans* rhodopsin is formed by 200 fs, after photoexcitation of the chromophore, in good agreement with spectroscopic data [10–12], and previous simulations [38,39]. The underlying mechanism, during this early time, involves direct nonadiabatic transfer from *cis* configurations in the S_1 state to *trans* configurations in the S_0 state, as illustrated in Fig. 3. At later times, there is partial reverse reaction reforming *cis* configurations in highly excited vibronic states.

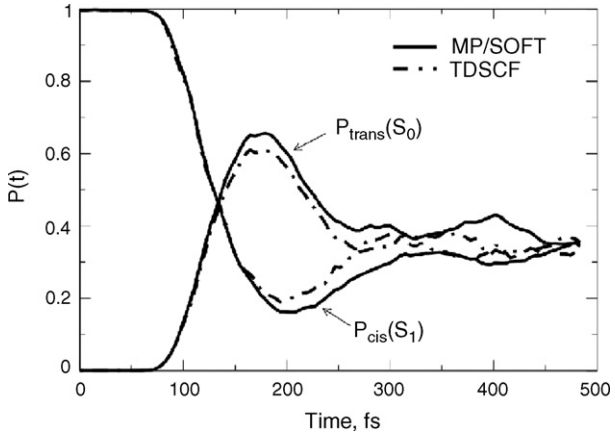

Fig. 4. Time-dependent populations of the 11-*cis* and all-*trans* configurations as a function of time, during the early time relaxation dynamics.

The quantitative comparison of time-dependent populations computed at the MP/SOFT and TDSCF levels of theory, partially validates the approximate mixed quantum-classical methodology as applied to the description of 11-*cis*/all-*trans* isomerization of rhodopsin provided by the 2-state 25-mode model Hamiltonian.

4. Concluding remarks

In this paper we have over-viewed the MP/SOFT method for simulations of nonadiabatic quantum dynamics in multi-dimensional (polyatomic) systems. We have shown that the MP/SOFT propagation scheme recursively applies the time-evolution operator, as defined by the Trotter expansion to second order accuracy, in dynamically adaptive coherent-state expansions generated according to the matching-pursuit algorithm. Such representations are particularly suitable for applications

to high-dimensional problems since they allow for an analytic implementation of the Trotter expansion, bypassing the exponential scaling problem associated with the usual fast-Fourier transform in the standard grid-based SOFT approach.

We have shown how to apply the MP/SOFT method to the description of the 11-*cis*/all-*trans* photoisomerization of the retinyl chromophore in rhodopsin, as modeled by a 2-state 25-dimensional wave-packet evolving according to an empirical Hamiltonian with frequencies and excited-state gradients parameterized to reproduce the observed resonance Raman excitations of rhodopsin.

The reported results provided a characterization of the reaction time and the detailed mechanism of isomerization as determined by the nonadiabatic dynamics at the S_0/S_1 conical intersection of potential energy surfaces. Direct comparisons of results for time-dependent reactant (product) populations computed according to the MP/SOFT methodology and the approximate TDSCF method have assessed the validity of a mixed quantum-classical approach as applied to the description of complex (nonintegrable) quantum dynamics in the multidimensional model systems defined by the 2-state 25-model Hamiltonian.

Acknowledgments

V.S.B. acknowledges a generous allocation of supercomputer time from the National Energy Research Scientific Computing (NERSC) center and financial support from Research Corporation, Research Innovation Award # RI0702, a Petroleum Research Fund Award from the American Chemical Society PRF # 37789-G6, a junior faculty award from the F. Warren Hellman Family, the National Science Foundation (NSF) Career Program Award CHE # 0345984, the NSF Nanoscale Exploratory Research (NER) Award ECS # 0404191, the Alfred P. Sloan Fellowship (2005–2006), a Camille Dreyfus Teacher-Scholar Award for 2005, and a Yale Junior Faculty Fellowship in the Natural Sciences (2005–2006).

References

[1] X. Chen, V.S. Batista. Matching-pursuit split operator Fourier transform simulations of excited-state nonadiabatic quantum dynamics in pyrazine. J. Chem. Phys., 125:Art. No. 124313, 2006.
[2] G. Wald, Molecular basis of visual excitation, Science 162 (1968) 230–239.
[3] C.R. Goldschmidt, M. Ottolenghi, T. Rosenfeld, Primary processes in photochemistry of rhodopsin at room-temperature, Nature 263 (1976) 169.
[4] T. Rosenfeld, B. Honig, M. Ottolenghi, J.B. Hurley, T.G. Ebrey, *cis–trans* isomerization in photochemistry of vision, Pure Appl. Chem. 49 (1977) 341.
[5] B. Honig, T.G. Ebrey, R.H. Callender, U. Dinur, R.H. Callender, Photoisomerization, energy-storage, and charge separation—model for light energy transduction in visual pigments and bacteriorhodopsin, Proc. Natl. Acad. Sci. U.S.A. 76 (1979) 2503.
[6] T. Ebrey, Y. Koutalos, Vertebrate photoreceptors, Prog. Retin. Eye Res. 20 (2001) 49.
[7] S.T. Menon, M. Han, T.P. Sakmar, Rhodopsin: structural basis of molecular physiology, Physiol. Rev. 81 (2001) 1659.
[8] T.P. Sakmar, R.R. Franke, H.G. Khorana, Glutamic acid-113 serves as the retinylidene schiff-base counterion in bovine rhodopsin, Proc. Natl. Acad. Sci. U.S.A. 86 (1989) 8309.
[9] T. Okada, O.P. Ernst, K. Palczewski, K.P. Hofmann, Activation of rhodopsin: new insights from structural and biochemical studies, Trends Biochem. Sci. 26 (2001) 318.
[10] Q. Wang, R.W. Schoenlein, L.A. Peteanu, R.A. Mathies, C.V. Shank, Vibrationally coherent photochemistry in the femtosecond primary event of vision, Science 266 (1994) 422.
[11] G.G. Kochendoerfer, R.A. Mathies, Spontaneous emission study of the femtosecond isomerization dynamics of rhodopsin, J. Phys. Chem. 100 (1996) 14526.
[12] R.W. Schoenlein, L.A. Peteanu, R.A. Mathies, C.V. Shank, The 1st step in vision—femtosecond isomerization of rhodopsin, Science 254 (1991) 412.
[13] A. Warshel, M. Karplus, Calculation of π–π^* excited state conformations and vibronic structure of retinal and related molecules, J. Am. Chem. Soc. 96 (1974) 5677.
[14] A. Warshel, Bicycle-pedal model for 1st step in vision process, Nature 260 (1976) 679.
[15] R.M. Weiss, A. Warshel, A new view of the dynamics of singlet *cis–trans* photoisomerization, J. Am. Chem. Soc. 101 (1979) 6131.
[16] A. Warshel, N. Barboy, Energy-storage and reaction pathways in the 1st step of the vision process, J. Am. Chem. Soc. 104 (1982) 1469.
[17] R.R. Birge, L.M. Hubbard, Molecular dynamics of *cis–trans* isomerization in rhodopsin, J. Am. Chem. Soc. 102 (1980) 2195.
[18] J.R. Tallent, E.W. Hyde, L.A. Findsen, G.C. Fox, R.R. Birge, Molecular dynamics of the primary photochemical event in rhodopsin, J. Am. Chem. Soc. 114 (1992) 1581.
[19] K. Palczewski, T. Kumasaka, T. Hori, C.A. Behnke, H. Motoshima, B.A. Fox, I. Le Trong, D.C. Teller, T. Okada, R.E. Stenkamp, M. Yamamoto, M. Miyano, Crystal structure of rhodopsin: a G protein-coupled receptor, Science 289 (2000) 739.
[20] D.C. Teller, T. Okada, C.A. Behnke, K. Palczewki, R.E. Stenkamp, Advances in determination of a high-resolution three-dimensional structure of rhodopsin, a model of G-protein-coupled receptors (GPCRs), Biochemistry 40 (2001) 7761.
[21] T. Okada, Y. Yoshinori, M. Silow, J. Navarro, J.N. Landau, Y. Schichida, Functional role of internal water molecules in rhodopsin revealed by X-ray crystallography, Proc. Natl. Acad. Sci. 99 (2002) 5982.
[22] M. Sugihara, V. Buss, P. Entel, M. Elstner, T. Frauenheim, 11-*cis*-retinal protonated Schiff base: influence of the protein environment on the geometry of the rhodopsin chromophore, Biochemistry 41 (2002) 15259.
[23] M. Sugihara, P. Entel, V. Buss, A first-principles study of 11-*cis*-retinal: modelling the chromophore–protein interaction in rhodopsin, Phase Transit. 75 (2002) 11.
[24] U.F. Rohrig, L. Guidoni, U. Rothlisberger, Early steps of the intramolecular signal transduction in rhodopsin explored by molecular dynamics simulations, Biochemistry 41 (2002) 10799.
[25] A. Yamada, T. Kakitani, S. Yamamoto, T. Yamato, A computational study on the stability of the protonated Schiff base of retinal in rhodopsin, Chem. Phys. Lett. 366 (2002) 670.
[26] N. Ferre, M. Olivucci, Probing the rhodopsin cavity with reduced retinal models at the CASPT2//CASSCF/AMBER level of theory, J. Am. Chem. Soc. 125 (2003) 6868.
[27] J.A. Gascon, V.S. Batista, QM/MM study of energy storage and molecular rearrangements due to the primary event in vision, Biophys. J. 87 (2004) 2931–2941.
[28] J.A. Gascon, E.M. Sproviero, V.S. Batista, QM/MM study of the NMR spectroscopy of the retinylidene chromophore in visual rhodopsin, J. Chem. Theor. Comput. 1 (2005) 674–685.
[29] J.A. Gascon, E.M. Sproviero, V.S. Batista, Computational studies of the primary phototransduction event in visual rhodopsin, Acc. Chem. Res. 39 (2006) 184–193.
[30] P.B. Coto, A. Sinicropi, L. De Vico, N. Ferre, M. Olivucci, Characterization of the conical intersection of the visual pigment rhodopsin at the CASPT2//CASSCF/AMBER level of theory, Mol. Phys. 104 (2006) 983–991.

[31] M. Olivucci, A. Lami, F. Santoro, A tiny excited-state barrier can induce a multiexponential decay of the retinal chromophore: a quantum dynamics investigation, Ang. Chem. Int. 44 (2005) 5118–5121.
[32] T. Vreven, F. Bernardi, M. Garavelli, M. Olivucci, M.A. Robb, H.B. Schlegel, Ab initio photoisomerization dynamics of a simple retinal chromophore model, J. Am. Chem. Soc. 119 (1997) 12687.
[33] M. Garavelli, T. Vreven, P. Celani, F. Bernardi, M.A. Robb, M. Olivucci, Photoisomerization path for a realistic retinal chromophore model: the nonatetraeniminium cation, J. Am. Chem. Soc. 120 (1998) 1285.
[34] M. Ben-Nun, T.J. Martinez, Electronic energy funnels in *cis–trans* photoisomerization of retinal protonated Schiff base, J. Phys. Chem. A 102 (1998) 9607.
[35] G. La Penna, F. Buda, A. Bifone, H.J.M. de, Groot, The transition state in the isomerization of rhodopsin, Chem. Phys. Lett. 294 (1998) 447.
[36] M. Garavelli, F. Bernardi, M.A. Robb, M. Olivucci, The shortchain acroleini-minium and pentadieniminium cations: towards a model for retinal photoisomerization. A CASSCF/PT2 study, J. Mol. Struc. Theochem. 463 (1999) 59.
[37] C. Molteni, I. Frank, M. Parrinello, An excited state density functional theory study of the rhodopsin chromophore, J. Am. Chem. Soc. 121 (1999) 12177.
[38] S. Hahn, G. Stock, Quantum-mechanical modeling of the femtosecond isomerization in rhodopsin, J. Phys. Chem. B 104 (2000) 1146.
[39] S.C. Flores, V.S. Batista, Model study of coherent-control of the femtosecond primary event of vision, J. Phys. Chem. B 108 (2004) 6745–6749.
[40] I. Burghardt, L.S. Cederbaum, J.T. Hynes, Environmental effects on a conical intersection: A model study, Faraday Discuss. 127 (2004) 395–411.
[41] M. Thoss, H.B. Wang, Quantum dynamical simulation of ultrafast molecular processes in the condensed phase, Mol. Phys. 322 (2006) 210–222.
[42] S.M. Lin, M. Groesbeek, I. van-der Hoef, P. Verdegem, J. Lugtenburg, R.A. Mathies, Vibrational assignment of torsional normal modes of rhodops Probing excited-state isomerization dynamics along the reactive $c-11=c-12$ torsion coordinate, J. Phys. Chem. B 102 (1998) 2787–2806.
[43] D. Neuhauser, Full quantal initial-state-selected reaction probabilities ($J=0$) for a 4-atom system- $H_2(v=0,1,\ J=0)+OH(v=0,\ 1,\ J=0)\rightarrow H+H_2O$, J. Chem. Phys. 100 (1994) 9272.
[44] W. Zhu, J.Z.H. Zhang, D.H. Zhang, Full-dimensional quantum dynamics calculation for D_2+CN reaction, Chem. Phys. Lett. 292 (1998) 46.
[45] G.C. Schatz, M.S. Fitzcharles, L.B. Harding, State-to-state chemistry with fast hydrogen atoms—reaction and collisional excitation in $H+CO_2$, Faraday Discuss. 84 (1987) 359.
[46] D.C. Clary, 4-atom reaction dynamics, J. Phys. Chem. 98 (1994) 10678.
[47] R. Kosloff, Propagation methods for quantum molecular dynamics, Annu. Rev. Phys. Chem. 45 (1994) 145.
[48] J.R. Fair, D. Schaefer, R. Kosloff, D.J. Nesbitt, Intramolecular energy flow and nonadiabaticity in vibrationally mediated chemistry: wave packet studies of $Cl+H_2O$, J. Chem. Phys. 116 (2002) 1406.
[49] J. Echave, D.C. Clary, Quantum-theory of planar 4-atom reactions, J. Chem. Phys. 100 (1994) 402.
[50] H.G. Yu, J.T. Muckerman, Quantum dynamics of the photoinitiated unimolecular dissociation of HOCO, J. Chem. Phys. 117 (2002) 11139.
[51] M.I. Hernandez, D.C. Clary, A study of HOCO resonances in the $OH+CO\rightarrow CO_2+H$ reaction, J. Chem. Phys. 101 (1994) 2779.
[52] D. Charlo, D.C. Clary, Quantum-mechanical calculations on termolecular association reactions $XY+Z+M\rightarrow XYZ+M$: application to ozone formation, J. Chem. Phys. 117 (2002) 1660.
[53] J.M. Bowman, Resonances: bridge between spectroscopy and dynamics, J. Phys. Chem. A 102 (1998) 3006.
[54] D.Q. Xie, R.Q. Chen, H. Guo, Comparison of Chebyshev, Faber, and Lanczos propagation-based methods for calculating resonances, J. Chem. Phys. 112 (2000) 5263.
[55] S.M. Anderson, T.J. Park, D. Neuhauser, Local propagating Gaussians: flexible vs. frozen widths, Phys. Chem. Chem. Phys. 1 (1999) 1343.
[56] M.D. Feit, J.A. Fleck Jr., A. Steiger, Solution of the Schrödinger-equation by a spectral method, J. Comput. Phys. 47 (1982) 412.
[57] M.D. Feit, J.A. Fleck Jr., A. Steiger, Solution of the Schrödinger equation by a spectral method. II. Vibrational energy levels of triatomic molecules, J. Chem. Phys. 78 (1983) 301.
[58] D. Kosloff, R. Kosloff, A Fourier method solution for the time-dependent Schrödinger-equation as a tool in molecular-dynamics, J. Comput. Phys. 52 (1983) 35.
[59] H. Tal-Ezer, R. Kosloff, An accurate and efficient scheme for propagating the time-dependent Schrödinger equation, J. Chem. Phys. 81 (1984) 3967–3971.
[60] T.J. Park, J.C. Light, Unitary quantum time evolution by iterative Lanczos reduction, J. Chem. Phys. 85 (1986) 5870–5876.
[61] R.K. Preston, J.C. Tully, Effects of surface crossing in chemical reactions—H_3^+ system, J. Chem. Phys. 54 (1971) 4297.
[62] J.C. Tully, Molecular dynamics with electronic transitions, J. Chem. Phys. 93 (1990) 1061.
[63] R.B. Gerber, V. Buch, M.A. Ratner, Time-dependent self-consistent field approximation for intramolecular energy transfer. 1. Formulation and application to dissociation and Van-der-Waals molecules, J. Chem. Phys. 77 (1982) 3022–3030.
[64] H.D. Meyer, W.H. Miller, A classical analog for electronic degrees of freedom in non-adiabatic collision processes, J. Chem. Phys. 70 (1979) 3214–3223.
[65] X. Sun, W.H. Miller, Semiclassical initial value representation for electronically non-adiabatic molecular dynamics, J. Chem. Phys. 106 (1997) 6346–6353.
[66] M. Thoss, G. Stock, Mapping approach to the semiclassical description of non-adiabatic quantum dynamics, Phys. Rev. A 59 (1999) 64.
[67] M.F. Herman, E. Kluk, A semiclassical justification for the use of non-spreading wavepackets in dynamics calculations, Chem. Phys. 91 (1984) 27.
[68] E. Kluk, M.F. Herman, H.L. Davis, Comparison of the propagation of semiclassical frozen Gaussian wave-functions with quantum propagation for a highly excited anharmonic-oscillator, J. Chem. Phys. 84 (1986) 326–334.
[69] G. Yang, M.F. Herman, Semiclassical surface hopping h–k propagator: application to two-dimensional, two-surface problems, J. Phys. Chem. B 105 (2001) 6562.
[70] F. Webster, P.J. Rossky, R.A. Friesner, Nonadiabatic processes in condensed matter: semi-classical theory and implementation, Comput. Phys. Commun. 63 (1991) 494.
[71] O.V. Prezhdo, P.J. Rossky, Mean-field molecular dynamics with surface hopping, J. Chem. Phys. 107 (1997) 825.
[72] D.F. Coker, Computer simulation of nonadiabatic dynamics in condensed systems, in: M.P. Allen, D.J. Tildesley (Eds.), Computer Simulation in Chemical Physics, Kluwer Academic Publishers, Dordrecht, 1993, pp. 315–377.
[73] S. Hammes-Schiffer, Multiconfigurational molecular-dynamics with quantum transitions: multiple proton-transfer reactions, J. Chem. Phys. 105 (1996) 2236.
[74] S. Hammes-Schiffer, J.C. Tully, Nonadiabatic infrequent events, J. Chem. Phys. 103 (1995) 8528.
[75] N. Makri, W.H. Miller, A semiclassical tunneling model for use in classical trajectory simulations, J. Chem. Phys. 91 (1989) 4026.
[76] A. Raab, G.A. Worth, H.D. Meyer, L.S. Cederbaum, Molecular dynamics of pyrazine after excitation to the s_2 electronic state using a realistic 24-mode model Hamiltonian, J. Chem. Phys. 110 (1999) 936–946.
[77] M. Thoss, W.H. Miller, G. Stock, Semiclassical description of nonadiabatic quantum dynamics: application to the S1–S2 conical intersection in pyrazine, J. Chem. Phys. 112 (2000) 10282–10292.
[78] M. Ben-Nun, T.J. Martinez, Nonadiabatic molecular dynamics validation of the multiple spawning method for a multi-dimensional problem, J. Chem. Phys. 108 (1998) 7244.
[79] M. Ben-Nun, T.J. Martinez, Ab initio quantum molecular dynamics, Adv. Chem. Phys. 121 (2002) 439.
[80] C. Coletti, G.D. Billing, Quantum dressed classical mechanics: application to the photo-absorption of pyrazine, Chem. Phys. Lett. 368 (2003) 289–298.

[81] D.V. Shalashilin, M.S. Child, Real time quantum propagation on a Monte Carlo trajectory guided grids of coupled coherent states: 26d simulation of pyrazine absorption spectrum, J. Chem. Phys. 121 (2004) 3563–3568.
[82] Y. Wu, V.S. Batista, Matching pursuit for simulations of quantum processes, J. Chem. Phys. 118 (2003) 6720.
[83] Y. Wu, V.S. Batista, Erratum: Matching pursuit for simulations of quantum processes [J. Chem. Phys.118, 6720, 2003], by yinghua wu and victor s. batista, J. Chem. Phys. 119 (2003) 7606.
[84] Y. Wu, V.S. Batista, Quantum tunneling dynamics in multidimensional systems: a matching-pursuit description, J. Chem. Phys. 121 (2004) 1676.
[85] X. Chen, Y. Wu, V.S. Batista, Matching-pursuit split operator Fourier transform computations of thermal correlation functions, J. Chem. Phys. 122 (2005) 64102.
[86] Y. Wu, M.F. Herman, V.S. Batista, Matching-pursuit split operator Fourier transform simulations of nonadiabatic quantum dynamics, J. Chem. Phys. 122 (2005) 114114.
[87] Y. Wu, V.S. Batista, Matching pursuit split operator Fourier transform simulations of excited-state intramolecular proton transfer in 2-(2′-hydroxyphenyl)-oxazole, J. Chem. Phys. 124 (2006), Art. No. 224305.
[88] W.H. Press, B.P. Flannery, S.A. Teukolsky, W.T. Vetterling, In Numerical Recipes, Cambridge University Press, Cambridge, 1986 (Chapter 12).
[89] I. Burghardt, H.D. Meyer, L.S. Cederbaum, Approaches to the approximate treatment of complex molecular systems by the multiconfiguration time-dependent hartree method, J. Chem. Phys. 111 (1999) 2927–2939.
[90] M.H. Beck, A. Jackle, G.A. Worth, H.D. Meyer, The multiconfiguration time-dependent Hartree (MCTDH) method: a highly efficient algorithm for propagating wavepackets, Phys. Rep. Rev. Sec. Phys. Lett. 324 (2000) 1.
[91] E.J. Heller, Wavepacket path integral formation of semiclassical dynamics, Chem. Phys. Lett. 34 (1975) 321–325.
[92] M.J. Davis, E.J. Heller, Semi-classical Gaussian-basis set method for molecular vibrational wave-functions, J. Chem. Phys. 71 (1979) 3383.
[93] E.J. Heller, Frozen Gaussians: a very simple semiclassical approximation, J. Chem. Phys. 75 (1981) 2923–2931.
[94] R.D. Coalson, M. Karplus, Extended wave packet dynamics; exact solution for collinear atom, diatomic molecule scattering, Chem. Phys. Lett. 90 (1982) 301.
[95] S.I. Sawada, R. Heather, B. Jackson, H. Metiu, A strategy for time-dependent quantum-mechanical calculations using a Gaussian wave packet representation of the wave-function, Chem. Phys. Lett. 83 (1985) 3009.
[96] K.G. Kay, Improved semiclassical propagation of wave packets, J. Chem. Phys. 91 (1989) 107.
[97] K. Thompson, T.J. Martinez, Ab initio/interpolated quantum dynamics on coupled electronic states with full configuration interaction wavefunctions, J. Chem. Phys. 110 (1999) 1376.
[98] J.D. Coe, T.J. Martinez, Competitive decay at two- and three-state conical intersections in excited-state intramolecular proton transfer, J. Am. Chem. Soc. 127 (2005) 4560–4561.
[99] J.D. Coe, T.J. Martinez, Ab initio molecular dynamics of excited-state intramolecular proton transfer around a three-state conical intersection in malonaldehyde, J. Chem. Phys. 110 (2006) 618–630.
[100] D.V. Shalashilin, B. Jackson, Initial value representation for the classical propagator and S-matrix with the help of coherent states, Chem. Phys. Lett. 291 (1998) 143.
[101] L.M. Andersson, Quantum dynamics using a discretized coherent state representation: an adaptive phase space method, J. Chem. Phys. 115 (2001) 1158–1165.
[102] D.V. Shalashilin, M.S. Child, Time dependent quantum propagation in phase space, J. Chem. Phys. 113 (2000) 10028.
[103] D.V. Shalashilin, M.S. Child, Multidimensional quantum propagation with the help of coupled coherent states, J. Chem. Phys. 115 (2001) 5367.
[104] G.A. Worth, I. Burghardt, Full quantum mechanical molecular dynamics using Gaussian wavepackets, Chem. Phys. Lett. 368 (2003) 502–508.
[105] G.A. Worth, M.A. Robb, I. Burghardt, A novel algorithm for non-adiabatic direct dynamics using variational Gaussian wavepackets, Faraday Discuss. 127 (2004) 307–323.
[106] S.G. Mallat, Z.F. Zhang, Matching pursuits with time-frequency dictionaries, IEEE T. Signal Process. 41 (1993) 3397.
[107] http://www-unix.mcs.anl.gov/mpi/http://www-unix.mcs.anl.gov/mpi/tutorial/gropp/talk.html.
[108] L. Seidner, W. Domcke, Microscopic modelling of photoisomerization and internal-conversion dynamics, Chem. Phys. 186 (1994) 27–40.
[109] L. Seidner, G. Stock, W. Domcke, Nonperturbative approach to femtosecond spectroscopy: general theory and application to multidimensional nonadiabatic photoisomerization processes, J. Chem. Phys. 103 (1995) 3998–4011.
[110] S. Hahn, G. Stock, Femtosecond secondary emission arising from the nonadiabatic photoisomerization in rhodopsin, Chem. Phys. 259 (297) (2000).